Title

Gripping Aerial Topology Optimized Robot (GATOR)

Authors

Guibert, Alexandre T
Chambers, Robert J
Cao, Pengcheng
et al.

Publication Date

2023-03-11

DOI

10.1109/aero55745.2023.10115720

Gripping Aerial Topology Optimized Robot (GATOR)

Alexandre T. Guibert[1]
Structural Engineering dept.
University of California San Diego
San Diego, USA
aguibert@ucsd.edu

Robert J. Chambers[1]
Material Science and Engineering dept.
University of California San Diego
San Diego, USA
rjchambers@ucsd.edu

Pengcheng Cao
Mechanical and Aerospace Engineering dept.
University of California San Diego
San Diego, USA
p5cao@eng.ucsd.edu

H. Alicia Kim
Structural Engineering dept.
University of California San Diego
San Diego, USA
hak113@eng.ucsd.edu

Shengqiang Cai
Mechanical and Aerospace Engineering dept.
University of California San Diego
San Diego, USA
shqcai@ucsd.edu

Falko Kuester
Computer Science and Engineering dept.
University of California San Diego
San Diego, USA
fkuester@ucsd.edu

***Abstract*— This paper introduces the design, modeling, manufacturing, and testing of a Gripping Aerial Topology Optimized Robot (GATOR). The airframe of this unmanned aerial vehicle (UAV) is designed to be lightweight, structurally stiff, modular, and multi-functional. A Level-Set Topology Optimization (LSTO) method defines the external geometry of the frame, while the frame infill is controlled using a variable thickness latticing technique based on Finite Element Analysis (FEA) results. The UAV incorporates a soft robotic gripper, allowing the vehicle to collect delicate samples from the environment and perch for low-power use for extended periods. The bio-inspired design and fabrication of a mountable soft robotic gripper are presented and the associated kinematics are derived for controls. To further decrease the weight of the designs a novel volume-changing material was introduced following careful characterization through Scanning Electron Microscopy (SEM) and tensile testing. The resulting platform leverages additive manufacturing using material extrusion technology and can be swiftly instrumented with propulsion and flight control systems. The presented modular design methodology can be applied to the rapid prototyping of a broad range of aerial platforms and lightweight structures.**

TABLE OF CONTENTS

1. INTRODUCTION

In recent years the small unmanned aerial systems (sUAS), as a subcategory of unmanned aerial vehicles (UAV), have been widely deployed to provide sensor support or perform aerial manipulation in many tasks. Their applications as pilot-controlled or fully automated sensor platforms include ecological monitoring [1], aerial imaging [2, 3], structural health monitoring [4, 5], and cultural heritage protection [6–8]. In some other tasks, the sUAS are required to physically interact with the environment with one or more robotic arms or end-effectors, which is generally categorized as aerial manipulation [9]. These tasks include grasping objects [10, 11], actively collecting samples from the field [12–14], and even extraterrestrial exploration [15, 16].

In order to realize certain objectives that enable the UAV to better serve the tasks, a number of design optimizations have been formulated and studied. For multirotor UAVs, airframe-related optimizations have been conducted to provide better flight maneuverability or dynamic performance. Strawson et al. [17, 18] studied the optimization of the rotor orientation of a fully-actuated hexrotor in order to generate the desired aerodynamic wrench profile. Magnussen et al. [19] presented a multirotor design optimization process to select optimal combinations of hardware under 4, 6 and 8-motor configurations. Additionally, topology optimization (TO) has been implemented for UAV airframe design. Martinez Leon et al. [20] implemented a structural-mechanical optimization for a composite quadrotor airframe using a generative design algorithm. Yap et al. [21] first characterized Nylon-12 filament for fabricating 3D printed quad-rotor airframe and then produced a topology-optimized airframe structure followed by finite element analysis (FEA) and loading tests. However, most TO methods used for multirotor design, e.g. those in [20, 21], are density-based methods available in commercial software. Such methods are known to render unmanufacturable structures and generally requires post-processing which can cost the optimality of the original solutions [22].

For the sUAS designed to perform aerial manipulation or perching, soft grippers have become an emerging design topic being frequently studied. Garcia Rubiales et al. [23] designed a soft gripper equipped on a hexrotor to perch on and crawl along a pipe for contact inspection. Ramon-Soria et al. [24] also presented a gripper hexrotor design to perch on and inspect the target pipe. However, both designs have a relatively heavy payload (346 g in [24]) or gross take-off weight (GTOW, 3.25 kg in [23]), which requires 6 or more rotors to provide enough lift for the system to stay airborne but can shorten the flight time and lower its energy efficiency. Fishman et al. [25] built a quadrotor platform with a soft gripper consisting of 4 lightweight silicone rubber fingers to

[1]These authors contributed equally to this work.

perform dynamic grasping. This gripper design, however, involves both injection molded fingers and 3D printed base plate and winch requiring extra time and effort for fabrication.

This paper presents a 3D printable lightweight quadrotor design with grasping capabilities to propose a solution to aforementioned issues in peers' work. The primary contributions of this paper are as follows: first, we performed both microscopic investigation using SEM and macroscopic testing via tensile experiments to characterize and select 3D printable materials for fabrication. Second, we developed a kinematically optimized lightweight compliant gripper design (148 g with a servo motor) which can be easily manufactured via 3D printing. Third, we invented a workflow of stress-based latticing techniques using a level-set method (LSM) to produce lightweight, stiff and manufacturable modular airframe components. Last but not least, we validated this design via FEA structural analyses, tensile tests, and experimental flights with grasping tasks.

The paper is organized as follows: the material characterization is presented in 2 and the design of the soft gripper and its kinematics are discussed in 3. The optimization of the airframe and the level-set topology optimization method are presented in 4. The flight tests and validation of the design are shown in 5. Finally, conclusions are drawn in 6.

2. Material Selection and Characterization

Introduction to foaming PLA and TPU

Since the advent of stereolithography (SLA) in the 1980s, Additive manufacturing has expanded into a wide array of techniques including Fused Filament Fabrication (FFF), Selective Laser Melting/Sintering, Polyjet, Direct Ink Writing, Powder Bed Fusion, and more [26]. Each technology possesses its own strengths and weaknesses, such as resolution and speed. In all techniques, a form of energy (light, laser, thermal) cures, melts, or sinters material in a layer-by-layer fashion to construct the final geometry. Benefits over traditional subtractive manufacturing include the possibility for more intricate internal geometry, ingratiating multiple parts, and the potential for less wasted material.

Within each printing methodology, the available materials range from very stiff, to elastomer-like properties. Metals, ceramics, and polymers can all be processed through additive manufacturing. There have been cases where multiple material classes are combined into a single print. Often additives are included in the material to impart further functionality. For example, silver nanoparticles and carbon nanotubes have been added to polymer filaments to create conductive 3D printed elastic strain sensors [27]. Recently the ability to create lower density parts through generating porosity across length scales has become an active research area [28–31]. This project will explore the impact of a blowing agent in polylactic acid (PLA) and thermoplastic polyurthane (TPU) on factors like print quality and material properties. The foaming filaments could be used to lower the density of the printed parts, especially applicable to UAVs, where weight drives key performance metrics like flight time.

For the average consumer, hobbyist, or engineering student, FFF has the lowest barrier to entry. In this method, the thermoplastic filament is fed into a heated extruder attached to a CNC control axis that lays a plastic bead layer-by-layer to construct the geometry. Armed with modeling and slicing software, a spool of filament, and a printer, the user can go from a design idea to a physical product in minutes. This allows for both rapid prototyping and fabrication of final parts.

Process Parameter	Unactivated	Activated
Layer Height [mm]	0.2	0.4
Hot End Temperature [°C]	200	240
Nozzle Speed [mm/s]	30	30
Extrusion Multiplier [%]	100	60

Table 1: Print parameters for specimen fabrication

Tensile Tests

One of the known drawbacks of the FFF technique is the large dependence of mechanical properties on the process parameters used to fabricate the part [32]. To validate the filaments used in this project, tensile tests following ASTM D638 were carried out to determine three parameters: Young's modulus, yield strength, and elongation at break. The direction of the infill within the coupon was controlled with the slicing software Simplify3D. 0° and 90° correspond with filament running parallel and perpendicular to the gauge length respectively. The print parameters are shown in Table 1. Note in the activated parts the extrusion multiplier is decreased to 60%. Without the foaming behavior this setting would result in a under-extruded failed print.

The uniaxial tensile experiments were conducted using an Instron machine (5965 Dual Column Testing System, Instron). The dogbone geometry followed Type IV in ASTM D638 printed on the Raise3D Pro2 printer. The tensile tests were performed with a crosshead speed of 5mm/min. The tensile results are shown in Fig. 1. The error bars indicate one standard deviation in each direction, i.e., the size of each error bar is twice the standard deviation of the associated quantity.

The Young's Modulus as well as the yield strength decreased when the micro-spheres are activated at a temperature of 240 °C. In addition, the elongation at break is significantly increased and the density of the activated material is roughly half of the density of the non-activated LW-PLA.

Scanning Electron Microscopy

After tensile testing this material, We wanted to observe the microstructure of the activated prints. The porosity created with the expansion of the micro-spheres could explain the differences in the mechanical properties. The fracture surfaces were observed using SEM and the images are presented in Fig. 2. In the 200 °C-0° specimen, small spheres of 15 μm were measured with ImageJ. In the expanded state the pores have a diameter of approximately 100 μm. In the 240 °C-0° specimen, the gap between layers is visible. The concentration of these large defects could contribute to the variation in elongation at break of this sample variety. A large void generates a stress concentration within the gauge length of the tensile specimen that could lead to fracture.

3. Design of the Soft Gripper

Details on design

One of the first design choices that needed to be made regarded the powertrain of the soft gripper. Pneumatic systems commonly power soft grippers but require an air source, plumbing, and valves. The weight of these components adds

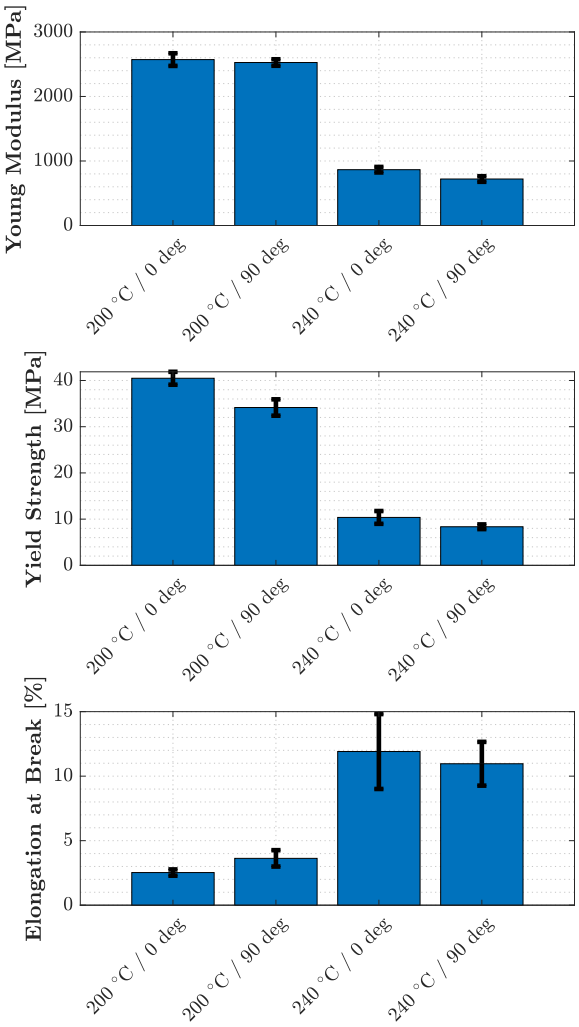

Figure 1: Results from tensile tests

up quickly, decreasing the potential flight time of the UAV. Rough order of magnitude calculations put this system in the range of 400g. Alternatively, the simplicity and low weight of a cable-driven design with one central servo motor drove the decision to pursue this configuration. A quality youtube video https://youtu.be/8F8gctNCGyE was used as inspiration for the first iteration of this design. The geometry of the gripper had many opportunities for creative design. Interesting features of the gripper include the use of the golden ratio in the digit length determination, texturing of the gripper surface, and creating a double curvature to allow for the gripper to act as landing gear. In an attempt to integrate bioinspiration into the design the golden ratio defined the digit lengths. This ratio manifests itself in countless patterns in nature such as the length of the digits on a human hand, nautilus shells, bighorn sheep horns, and spiraling galaxies [33]. When it tightens the gripper will form a logarithmic spiral, enabling a similar grip to a hand. The digit length was modeled in SolidWorks with equations to allow the user to tune the length to the desired dimensions.

One of the compelling features of the software package nTopology is the ability to easily apply texture to a surface and unite it with the original body. Texturing the gripper surface of a soft robotic gripper has been done frequently in the soft robotic field. The Bioinspired Robotics and Design Lab at UCSD commonly applies texture to their grippers [34,35]. The pattern depends on the target environment of the gripper, i.e. aquatic vs dry. To increase the friction between the gripper and its target object, a Voronoi surface texture was applied to the gripping surfaces using the software nTopology.

Another interesting aspect of the design was using a double curvature in the gripper leg to allow for the gripper to support weight when loaded from the bottom. The cable acts as a tendon creating tension and allowing the geometry to be self-supported. The thermally activated foaming TPU was used for printing the soft gripper. The extrusion mulitiplier was set to 80% for the TPU. To get a successful print with unactivated TPU, the multiplier needed to be set to 120%. This corresponds to a 33g weight difference between the activated and unactivated designs.

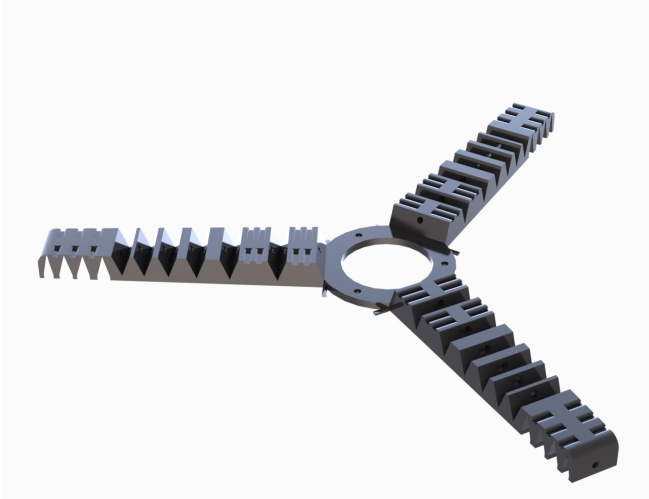

Figure 3: Planar Soft gripper design

Kinematics of the soft gripper

A kinematic study of linkage systems and the use of nonlinear optimization in MATLAB garner a better understanding of the shape the gripper will take given digit lengths and joint stiffness. Both of these parameters are easily modified within the CAD model. Before the nonlinear optimization can be run, the geometry of the system must be modeled, as shown in Fig. 4a. The red dots represent the guide holes, the green dotted line represents the cable and the solid blue lines represent the digit lengths. The vector $\overrightarrow{v}$ is defined as the distance between two guide holes.

The optimization function will be to minimize the strain energy of the system subject to the conservation of tendon line length. Where L_0 is the initial cable length and δ is the change in cable length. This formulation is shown in Eqn 1.

$$\begin{aligned} \underset{x}{\text{minimize}} \quad & \frac{1}{2}k_1\theta_1^2 + \frac{1}{2}k_2\theta_2^2 + \frac{1}{2}k_3\theta_3^2 + \frac{1}{2}k_4\theta_4^2 \\ \text{subject to} \quad & 0 = \|\overrightarrow{v_0}\| + \|\overrightarrow{v_1}\| + \|\overrightarrow{v_2}\| + \|\overrightarrow{v_3}\| - L_0 + \delta \end{aligned} \tag{1}$$

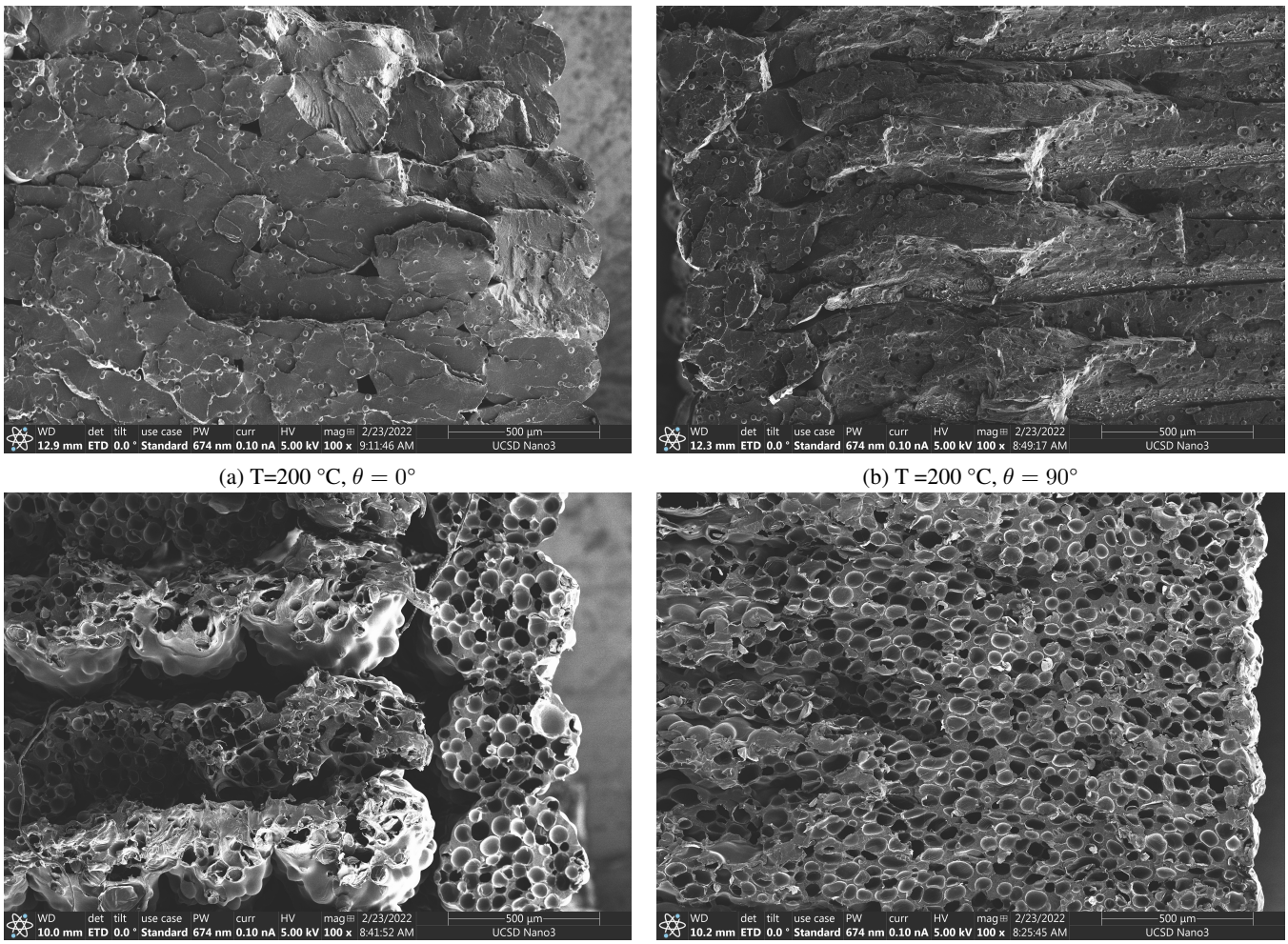

(a) T=200 °C, $\theta = 0°$

(b) T =200 °C, $\theta = 90°$

(c) T=240 °C, $\theta = 0°$

(d) T=240 °C, $\theta = 90°$

Figure 2: SEM images of LW-PLA fractured surfaces

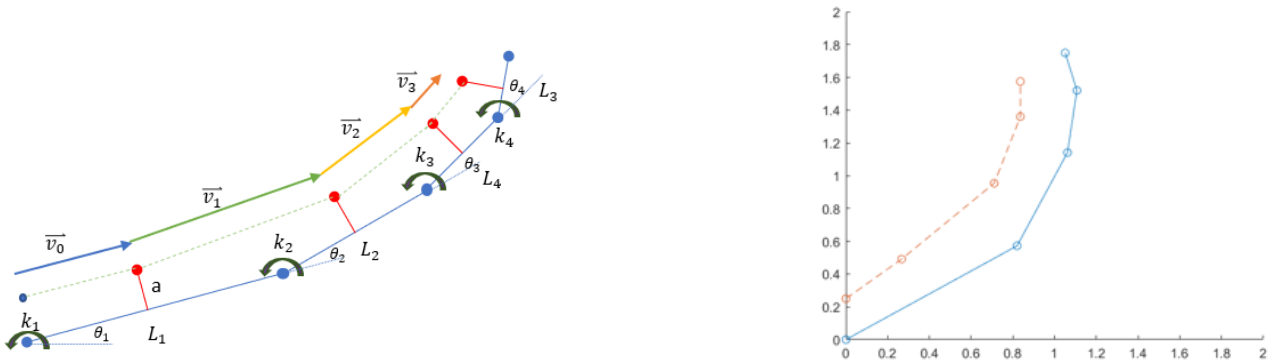

(a) Definition of model geometry

(b) MATLAB output

Figure 4: Kinematic study of soft gripper

The MATLAB function *fmincon* was used to calculate the angles of each joint. This implementation of *fmincon* finds the minimum of a constrained nonlinear multivariable function, subject to a nonlinear constraint. Fig 4b shows a plot generated for joint stiffnesses that decrease along the length of the finger. A possible use of this solver would be to tune the joint stiffnesses to achieve the desired deformed shape. In the 3D model, an increase in joint stiffness is related to an increase in the cross-sectional area of the joint. The geometry of the gripper could be modified if the goal payload was 2 cm vs 10 cm in diameter.

4. TOPOLOGY OPTIMIZATION OF THE AIRFRAME

Level-set method

Level-set topology optimization (LSTO) is a popular gradient-based optimization method. It aims at optimizing the material layout in a design domain for a specific set of load cases, objectives, and constraints. However, unlike density-based methods which are also popular gradient-based optimization methods that are usually found in commercial solutions, e.g., in Abaqus or nTopology, the level-set method does not require additional filtering techniques. Indeed, at any time, the boundary is implicitly defined and topological changes are handled naturally. The clear definition of the boundaries is appealing for design-dependent pressure loads as described in [36]. The level-set method was originally developed to track interfaces in the context of front propagation using a Hamilton-Jacobi equation [37]. Thus, level-set topology optimization is sometimes classified as a boundary-based method where the boundary of the structure is defined as the zero level-set of an implicit function ϕ such that:

$$\begin{cases} \phi(x) \geq 0, x \in \Omega \\ \phi(x) = 0, x \in \Gamma \\ \phi(x) < 0, x \notin \Omega \end{cases} \tag{2}$$

where Ω is the structure domain and Γ is the boundary. A signed-distance function is classically used to initialize ϕ [38]. The topology of the structure is optimized by iteratively solving the following Hamilton-Jacobi type of equation, so-called the level-set advection equation:

$$\frac{\partial \phi(x)}{\partial t} + |\nabla \phi(x)| V_n(x) = 0 \tag{3}$$

where t is a fictitious time domain and V_n is the normal velocity. The discretized form of this Hamilton-Jacobi equation is usually expressed as:

$$\phi_i^{k+1} = \phi_i^k - \Delta t |\nabla \phi_i^k| V_{n,i}^k \tag{4}$$

where k is the iteration number, i is a point in the domain, Δt is the time step, and $V_{n,i}$ is the normal velocity at the grid point i in the domain. The velocities are computed as a linear combination of the sensitivities of the objectives and constraints. In our approach, the sensitivities are computed using the discrete adjoint method via a local perturbation scheme. For more information regarding the discrete adjoint method, the reader is referred to [39]. In addition, the level-set method is described in details in [38] and [40]. The method is implemented using the framework presented in [41] where the optimization relies on in-house C++ code and uses FEniCS as a finite element solver [42, 43].

Problem setup

The airframe is composed of a flight deck and four arms. Each arm links a rotor to the flight deck. The arms only are optimized since the flight deck composed of the power supply and electronic components is bought off the shelf from ModalAI. For more information regarding ModalAI, please see https://www.modalai.com/. One arm is optimized and considered for the design domain. The optimized design will then be used for the four arms. The objective for the optimization of each arm is to minimize structural compliance to obtain a stiff structure. In addition, the volume should be constrained to obtain a lightweight arm. The problem is formulated as follows:

$$\begin{aligned} \underset{x}{\text{minimize}} \quad & \frac{1}{2} \int_\Omega \sigma : \epsilon \, d\Omega \\ \text{subject to} \quad & V \leq 0.06 \times V_0 \\ & \mathbf{K}U = F \end{aligned} \tag{5}$$

where σ and ϵ are the stress and strain tensors respectively, V is the volume of the structure, and V_0 is the volume of the design domain. $\mathbf{K}$ is the structural stiffness matrix, U is the vector of nodal displacements, and F is the vector of external forces. Note that linear elasticity was assumed. The volume fraction was chosen to be 0.06 to obtain a mass of less than 45g per arm.

The force induced by the rotors was applied on one side of the initial domain where the motor will be mounted. The magnitude of the force has been determined to be 10 N with thrust tests and is applied in an upward direction. The other side of the initial design is fixed using a homogeneous Dirichlet boundary condition. A 3D finite element mesh comprised of 53 x 33 x 13 cubic elements in the horizontal, vertical, and thickness direction respectively is used for the analysis. The initial design and boundary conditions are presented in Fig. 5.

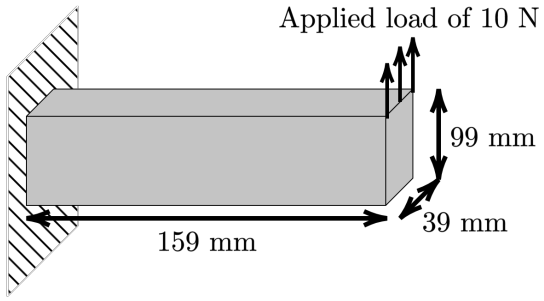

Figure 5: Arm optimization: initial design and boundary conditions

Proposed workflow and Lattice structure

The external geometry of the arm is obtained using the LSTO. Latticing techniques are used to control the interior geometry of the arm which will be the infill of the additively manufactured arm. The outer geometry from the LSTO results is preserved. The gyroid shape was chosen to be the unit cell for the lattice and the thickness of the gyroid walls is based on a

Finite Element Analysis (FEA). Indeed, the LSTO results are imported in nTopology where a first FEA is carried out. Then, a linear relationship between the von Mises stress distribution obtained from the FEA and the wall thickness of the unit cell is established. Where the stress is minimal, the thickness is minimal, i.e., 0.4 mm, and where the stress is maximal, the thickness is maximal, i.e., 0.8 mm. The thickness of the walls defining the external geometry is kept constant at 0.8 mm. Finally, before printing the geometry, another FEA is carried out to ensure that the maximum von Mises stress is less than the measured Yield stress of the material. The proposed workflow is presented in Fig. 6.

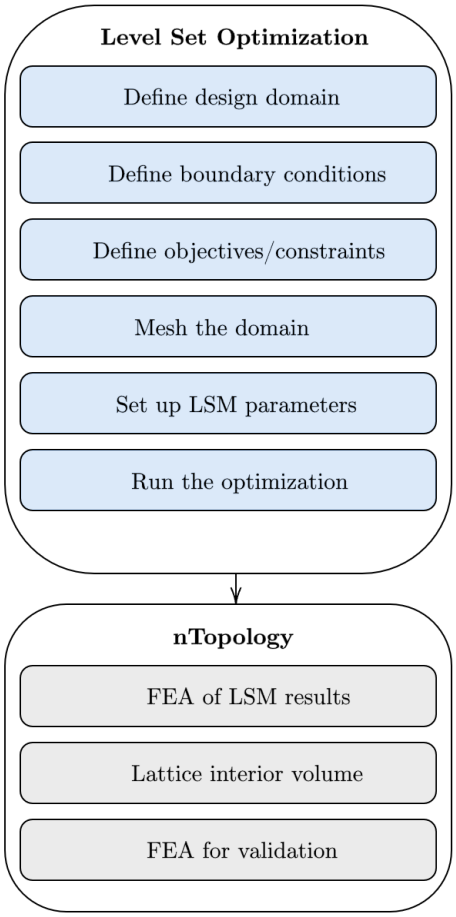

Figure 6: Proposed optimization workflow

The optimized arm is shown in Fig. 7. Note that the motor mount and the flight deck mount were added using Boolean union operations in nTopology after the part has been optimized. It is also possible to smooth the part by either using a finer mesh or by using post-processing software, e.g., MeshMixer.

5. Validation and Flight Tests

Validation of the arm with FEA and experiments

In this section, we compare the deflection predicted with FEA to experiments. An experimental rig was designed to measure the displacement of the tip of the arm when a load is applied using a dial gauge indicator. The design of the rig for testing the arm is presented in Fig. 8 where the typical design of an arm is shown in black. Masses up to 1.5kg were positioned on

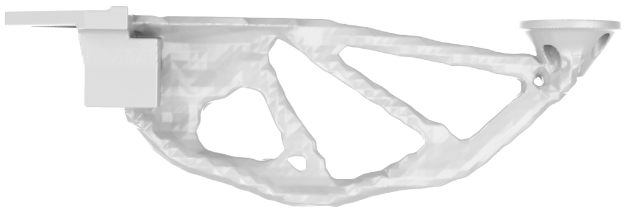

Figure 7: Optimization results

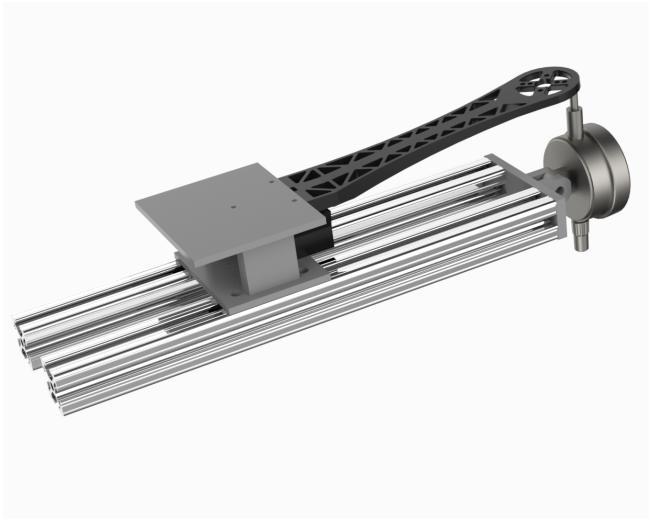

Figure 8: Experimental setup for testing the arm

the motor mount location and the displacement was recorded.

The part was analyzed using Intact.Simulation which uses a geometry moments-based technology. This method is especially appropriate for fine features such as a lattice infill and is the reason why it has been chosen. For more information, please refer to https://www.intact-solutions.com. The finite element results for a load of 10 N are presented in Fig. 9a. The maximum deflection obtained from the finite element analysis is compared to the experimental measurements in Fig. 9b. The discrepancies between the experiment and simulation might be explained by the isotropic and linear elasticity assumptions in the simulation. In addition, manufacturing variability is not considered in the FEA. However, the arm was able to consistently carry a load of ≈ 1.5 times its nominal load without any damage. Additional investigation and refinement of the finite element model are needed to explain these discrepancies and are beyond the scope of the current work.

Results from flights

A CAD rendering of the final assembly is presented in Fig. 10. The ModalAI m500 airframe was modified to integrate the optimized arms and soft gripper. M2.5 heat-set inserts were installed into the optimized arms to increase the robustness of attachment to the airframe. A Spektrum DX8 RC controller was paired and configured to the drone using

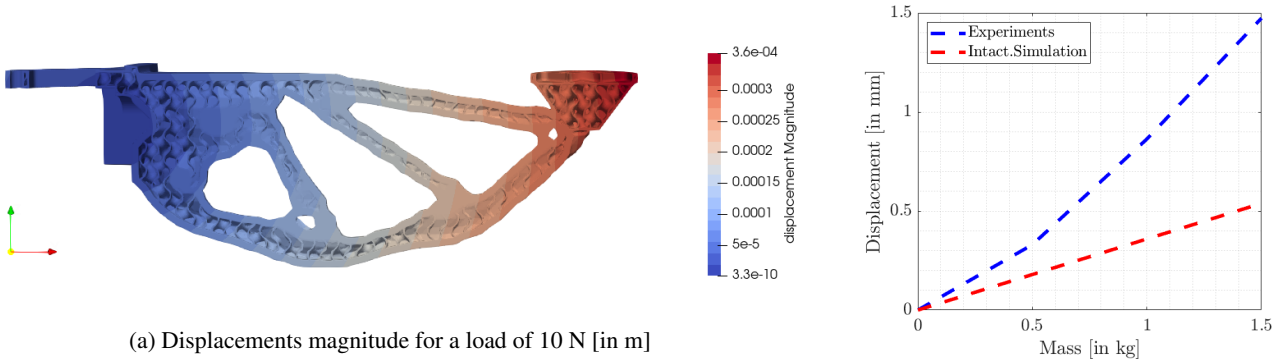

(a) Displacements magnitude for a load of 10 N [in m]

(b) Deflection results

Figure 9: Finite element analysis of the arm

QGround Control and the VOXL flight deck. One of the auxiliary channels on the PWM breakout board on the m500 was connected to the servomotor signal wire. The servo received power from a 16V to 5V regulator. The three flight modes in this UAV system are called *manual*, *position*, and *offboard*. The latter two flight modes use visual-inertial odometry data from the VOXL to control position. Three cameras and an inertial measurement unit on the controller make this possible. In *position* flight mode the UAV maintains a steady position until it receives commands from the RC controller, In *offboard* flight mode the drone flies in a Figure-8 pattern. All three of these flight modes were successfully tested with the UAV. Additionally, the gripping capability of the drone was successfully tested with objects of varying sizes and shapes. Fig. 10c shows the grasping sequence of the GATOR drone. The example payload in this demonstration was 74g.

6. Conclusions

Unmanned aerial vehicles have become an essential tool for remote exploration and data acquisition. In particular, UAV with soft gripping capabilities allow for the manipulation of fragile targets in difficult to reach areas. In this work, we presented the design, modeling, manufacturing, and testing of a gripping aerial topology optimized robot (GATOR) for such missions.

The conclusions of this research project are as follows. First, foaming PLA and TPU filaments for 3D-printing are introduced and adopted to save weight for the UAV. Through SEM and tensile tests, their material properties were studied with prints under different manufacturing conditions. Second, we presented the design of the soft gripper and the derived kinematics to control the rotation angles of each digit. This gripper was manufactured via a single print using TPU. Third, the level-set method was introduced and used to optimize the UAV frame. We proposed a reusable sequential optimization workflow based on topology optimization for rapid prototyping and deployment where finite element analysis, specifically the stress distribution, is utilized to control the infill of the additively manufactured part. Finally, displacements were measured to test the airframe's stiffness with an experimental setup. We tested GATOR in experimental flights and successfully performed gripping tasks for a payload of 74g. The UAV proved effective in gripping and carrying different objects. This analysis-driven design process including the validation is presented with the intent of inspiring our fellow researchers on novel UAV designs.

In addition, we believe that this study can be extended and future work will include:

- Multiscale topology optimization where the micro-scale, i.e. print porosity, meso-scale, i.e. lattice infill and the macro-scale, i.e. external geometry, are optimized simultaneously
- Multi-material topology optimization enabled by dual extrusion additive manufacturing
- Further characterization the relationship between microstructure and bulk properties of the foaming materials
- Application of the level-set method to optimize the soft-gripper
- Improvement and further investigation of the finite element model of the airframe
- Consideration of impact scenarios

Acknowledgment

This publication is based on work supported by the US Army Corps of Engineers under research Cooperative Agreement W912HZ-17-2-0024 and under the auspices of the U.S. Department of Energy by Lawrence Livermore National Laboratory under Contract DE-AC52-07NA27344 and by the LLNL-LDRD Program under Project No. 20-SI-005. Additional support was provided by the Kinsella Expedition Fund. We thank all collaborators at the Qualcomm Institute, the Departments of Mechanical, Structural Engineering, and Material Science, and the Contextual Robotics Institute, UC San Diego, as well as all other contributors to ideas, suggestions and comments. Opinions, findings, and conclusions from this study are those of the authors and do not necessarily reflect the opinions of the research sponsors.

References

[1] R. Díaz-Delgado and S. Mücher, "Editorial of special issue "drones for biodiversity conservation and ecological monitoring"," *Drones*, vol. 3, no. 2, p. 47, 2019.

[2] T. Wypych, J. Strawson, V. Petrovic, R. Angelo, A. Hoff, M. Howland, M. Seracini, T. Levy, and F. Kuester, "Airborne imaging for cultural heritage," in *2014 IEEE Aerospace Conference*. IEEE, 2014, pp. 1–9.

[3] C. A. F. Ezequiel, M. Cua, N. C. Libatique, G. L. Tangonan, R. Alampay, R. T. Labuguen, C. M. Favila,

(a) side view of the final design

(b) bottom view of the final design

(c) gripping sequence

Figure 10: Final design and flight test

J. L. E. Honrado, V. Canos, C. Devaney *et al.*, "Uav aerial imaging applications for post-disaster assessment, environmental management and infrastructure development," in *2014 International conference on unmanned aircraft systems (ICUAS)*. IEEE, 2014, pp. 274–283.

[4] S. Zhao, F. Kang, J. Li, and C. Ma, "Structural health monitoring and inspection of dams based on uav photogrammetry with image 3d reconstruction," *Automation in Construction*, vol. 130, p. 103832, 2021.

[5] S. Sankarasrinivasan, E. Balasubramanian, K. Karthik, U. Chandrasekar, and R. Gupta, "Health monitoring of civil structures with integrated uav and image processing system," *Procedia Computer Science*, vol. 54, pp. 508–515, 2015.

[6] W. Frodella, M. Elashvili, D. Spizzichino, G. Gigli, L. Adikashvili, N. Vacheishvili, G. Kirkitadze, A. Nadaraia, C. Margottini, and N. Casagli, "Combining infrared thermography and uav digital photogrammetry for the protection and conservation of rupestrian cultural heritage sites in georgia: A methodological application," *Remote Sensing*, vol. 12, no. 5, p. 892, 2020.

[7] A. Ulvi, "Documentation, three-dimensional (3d) modelling and visualization of cultural heritage by using unmanned aerial vehicle (uav) photogrammetry and terrestrial laser scanners," *International Journal of Remote Sensing*, vol. 42, no. 6, pp. 1994–2021, 2021.

[8] K. Themistocleous, "The use of uavs for cultural heritage and archaeology," in *Remote Sensing for Archaeology and Cultural Landscapes*. Springer, 2020, pp. 241–269.

[9] F. Ruggiero, V. Lippiello, and A. Ollero, "Aerial manipulation: A literature review," *IEEE Robotics and Automation Letters*, vol. 3, no. 3, pp. 1957–1964, 2018.

[10] P. E. Pounds, D. R. Bersak, and A. M. Dollar, "Grasping from the air: Hovering capture and load stability," in *2011 IEEE international conference on robotics and automation*. IEEE, 2011, pp. 2491–2498.

[11] D. Mellinger, Q. Lindsey, M. Shomin, and V. Kumar, "Design, modeling, estimation and control for aerial grasping and manipulation," in *2011 IEEE/RSJ International Conference on Intelligent Robots and Systems*. IEEE, 2011, pp. 2668–2673.

[12] C. Koparan, A. B. Koc, C. V. Privette, and C. B. Sawyer,

"Autonomous in situ measurements of noncontaminant water quality indicators and sample collection with a uav," *Water*, vol. 11, no. 3, p. 604, 2019.

[13] H. La Vigne, G. Charron, J. Rachiele-Tremblay, D. Rancourt, B. Nyberg, and A. Lussier Desbiens, "Collecting critically endangered cliff plants using a drone-based sampling manipulator," *Scientific Reports*, vol. 12, no. 1, pp. 1–11, 2022.

[14] G. Jiang, R. M. Voyles, and J. J. Choi, "Precision fully-actuated uav for visual and physical inspection of structures for nuclear decommissioning and search and rescue," in *2018 IEEE International Symposium on Safety, Security, and Rescue Robotics (SSRR)*. IEEE, 2018, pp. 1–7.

[15] L. A. Young, P. Lee, E. Aiken, G. Briggs, G. M. Pisanich, S. Withrow-Maser, and H. Cummings, "The future of rotorcraft and other aerial vehicles for mars exploration," in *Vertical Flight Society's 77th Annual Forum & Technology Display*, 2018.

[16] J. Balaram, M. Aung, and M. P. Golombek, "The ingenuity helicopter on the perseverance rover," *Space Science Reviews*, vol. 217, no. 4, pp. 1–11, 2021.

[17] J. Strawson, P. Cao, T. Bewley, and F. Kuester, "Rotor orientation optimization for direct 6 degree of freedom control of multirotors," in *2021 IEEE Aerospace Conference (50100)*. IEEE, 2021, pp. 1–12.

[18] J. Strawson, P. Cao, D. Tran, T. Bewley, and F. Kuester, "Monocoque multirotor airframe design with rotor orientations optimized for direct 6-dof uav flight control," in *AIAA AVIATION 2021 FORUM*, 2021, p. 2431.

[19] Ø. Magnussen, G. Hovland, and M. Ottestad, "Multicopter uav design optimization," in *2014 IEEE/ASME 10th International Conference on Mechatronic and Embedded Systems and Applications (MESA)*. IEEE, 2014, pp. 1–6.

[20] A. Martinez Leon, A. Rukavitsyn, and S. Jatsun, "Uav airframe topology optimization," in *International Conference on Industrial Engineering*. Springer, 2021, pp. 338–346.

[21] Y. L. Yap, W. Toh, A. Giam, F. R. Yong, K. I. Chan, J. W. S. Tay, S. S. Teong, R. Lin, and T. Y. Ng, "Topology optimization and 3d printing of micro-drone: Numerical design with experimental testing," *International Journal of Mechanical Sciences*, p. 107771, 2022.

[22] B. S. Lazarov, F. Wang, and O. Sigmund, "Length scale and manufacturability in density-based topology optimization," *Archive of Applied Mechanics*, vol. 86, no. 1, pp. 189–218, 2016.

[23] F. J. Garcia Rubiales, P. Ramon Soria, B. C. Arrue, and A. Ollero, "Soft-tentacle gripper for pipe crawling to inspect industrial facilities using uavs," *Sensors*, vol. 21, no. 12, p. 4142, 2021.

[24] P. Ramon-Soria, A. E. Gomez-Tamm, F. J. Garcia-Rubiales, B. C. Arrue, and A. Ollero, "Autonomous landing on pipes using soft gripper for inspection and maintenance in outdoor environments," in *2019 IEEE/RSJ International Conference on Intelligent Robots and Systems (IROS)*. IEEE, 2019, pp. 5832–5839.

[25] J. Fishman, S. Ubellacker, N. Hughes, and L. Carlone, "Dynamic grasping with a" soft" drone: From theory to practice," in *2021 IEEE/RSJ International Conference on Intelligent Robots and Systems (IROS)*. IEEE, 2021, pp. 4214–4221.

[26] A. Su and S. J. Al'Aref, "Chapter 1 - history of 3d printing," in *3D Printing Applications in Cardiovascular Medicine*, S. J. Al'Aref, B. Mosadegh, S. Dunham, and J. K. Min, Eds. Boston: Academic Press, 2018, pp. 1–10. [Online]. Available: https://www.sciencedirect.com/science/article/pii/B9780128039175000018

[27] D. Xiang, X. Zhang, E. Harkin-Jones, W. Zhu, Z. Zhou, Y. Shen, Y. Li, C. Zhao, and P. Wang, "Synergistic effects of hybrid conductive nanofillers on the performance of 3d printed highly elastic strain sensors," *Composites Part A: Applied Science and Manufacturing*, vol. 129, p. 105730, 2020. [Online]. Available: https://www.sciencedirect.com/science/article/pii/S1359835X19304798

[28] D. Tammaro, R. Della Gatta, M. M. Villone, and P. L. Maffettone, "Continuous 3d printing of hierarchically structured microfoamed objects," *Advanced Engineering Materials*, vol. 24, no. 5, p. 2101226, 2022.

[29] C. W. Visser, D. N. Amato, J. Mueller, and J. A. Lewis, "Architected polymer foams via direct bubble writing," *Advanced materials*, vol. 31, no. 46, p. 1904668, 2019.

[30] S. E. Seo, Y. Kwon, N. D. Dolinski, C. S. Sample, J. L. Self, C. M. Bates, M. T. Valentine, and C. J. Hawker, "Three-dimensional photochemical printing of thermally activated polymer foams," *ACS Applied Polymer Materials*, vol. 3, no. 10, pp. 4984–4991, 2021.

[31] D. M. Wirth, A. Jaquez, S. Gandarilla, J. D. Hochberg, D. C. Church, and J. K. Pokorski, "Highly expandable foam for lithographic 3d printing," *ACS applied materials & interfaces*, vol. 12, no. 16, pp. 19 033–19 043, 2020.

[32] S. Anand Kumar and Y. Shivraj Narayan, "Tensile testing and evaluation of 3d-printed PLA specimens as per ASTM d638 type IV standard," in *Innovative Design, Analysis and Development Practices in Aerospace and Automotive Engineering (I-DAD 2018)*, U. Chandrasekhar, L.-J. Yang, and S. Gowthaman, Eds. Springer Singapore, 2019, pp. 79–95, series Title: Lecture Notes in Mechanical Engineering. [Online]. Available: http://link.springer.com/10.1007/978-981-13-2718-6_9

[33] M. Akhtaruzzaman and A. A. Shafie, "Geometrical substantiation of phi, the golden ratio and the baroque of nature, architecture, design and engineering," *International Journal of Arts*, vol. 1, no. 1, pp. 1–22, 2011.

[34] P. Glick, S. A. Suresh, D. Ruffatto, M. Cutkosky, M. T. Tolley, and A. Parness, "A soft robotic gripper with gecko-inspired adhesive," *IEEE Robotics and Automation Letters*, vol. 3, no. 2, pp. 903–910, 2018.

[35] J. A. Sandoval, T. Xu, I. Adibnazari, D. D. Deheyn, and M. T. Tolley, "Combining suction and friction to stabilize a soft gripper to shear and normal forces, for manipulation of soft objects in wet environments," *IEEE Robotics and Automation Letters*, vol. 7, no. 2, pp. 4134–4141, 2022.

[36] A. Neofytou, R. Picelli, T.-H. Huang, J.-S. Chen, and H. A. Kim, "Level set topology optimization for design-dependent pressure loads using the reproducing kernel particle method," *Structural and Multidisciplinary Optimization*, vol. 61, no. 5, pp. 1805–1820, 2020.

[37] S. Osher and J. A. Sethian, "Fronts propagating with curvature-dependent speed: Algorithms based on hamilton-jacobi formulations," *Journal of computational physics*, vol. 79, no. 1, pp. 12–49, 1988.

[38] S. J. Osher and R. Fedkiw, *Level set methods and dynamic implicit surfaces.*, ser. Applied mathematical sciences. Springer, 2003, vol. 153.

[39] S. Kambampati, H. Chung, and H. A. Kim, "A discrete adjoint based level set topology optimization method for stress constraints," *Computer Methods in Applied Mechanics and Engineering*, vol. 377, p. 113563, 2021.

[40] P. D. Dunning and H. A. Kim, "Introducing the sequential linear programming level-set method for topology optimization," *Structural and Multidisciplinary Optimization*, vol. 51, no. 3, pp. 631–643, 2015. [Online]. Available: http://link.springer.com/10.1007/s00158-014-1174-z

[41] J. Hyun, C. Jauregui, H. A. Kim, and A. Neofytou, *On Development of an Accessible and non-Intrusive Level-set Topology Optimization Framework via the Discrete Adjoint Method*. AIAA, 2022. [Online]. Available: https://arc.aiaa.org/doi/abs/10.2514/6.2022-2548

[42] M. Alnæs, J. Blechta, J. Hake, A. Johansson, B. Kehlet, A. Logg, C. Richardson, J. Ring, M. E. Rognes, and G. N. Wells, "The fenics project version 1.5," *Archive of Numerical Software*, vol. 3, no. 100, 2015.

[43] G. W. Anders Logg, Kent-Andre Mardal, *Automated Solution of Differential Equations by the Finite Element Method*. Springer Berlin, Heidelberg, 2012.

BIOGRAPHY

Alexandre T. Guibert *is a Ph.D. Student in the Structural Engineering Department at the University of California San Diego (UCSD), San Diego, USA. He received an M.S. degree in Mechanical Engineering from the Polytechnic School of Orléans, France, and an M.S. degree in Fundamental and Applied Physics from the University of Orléans, France. He also earned a master's degree in Business Administration and Management from the Business Administration Institute of Orléans, France. His primary research interests cover the development of computational models and optimization algorithms for multiscale and multiphysics problems.*

Robert J. Chambers *is a Ph.D. Student in the Material Science and Engineering Department at the University of California San Diego, San Diego, USA. He received a Composites Engineering Certificate, Bachelors of Science in Mechanical Engineering and a Bachelors of Science in Business from the University of Connecticut. Before attending UCSD, he worked as a R&D engineer for GKN Aerospace from 2018 to 2021. His research interest include multi-material additive manufacturing and the impact of process parameters on the mechanical response of polymeric materials.*

Pengcheng Cao *received his BEng in Energy Engineering from Shandong University, China in 2016 and his MSc in Mechanical Engineering from the University of California, San Diego in 2018. He worked as a project engineer in Value Wholesaler Inc. in Duarte, CA in 2018 and is currently pursuing his Ph.D. in the Department of Mechanical Engineering at UC San Diego under the guidance of Prof. Falko Kuester and Prof. Thomas Bewley. His research interests lie in controls and dynamic systems, robotics, and photogrammetry.*

H. Alicia Kim *is a Professor in Structural and Material Optimization in the Structural Engineering Department of the University of California San Diego. Her interests are in level set topology optimization, multiscale and multiphysics optimization, modeling and optimization of composite materials and multifunctional structures. She has published nearly 200 journal and conference papers in these fields including award winning papers at the AIAA conferences and World Congresses on Structural and Multidisciplinary Optimization. She is a Review Editor for the Structural and Multidisciplinary Optimization journal.*

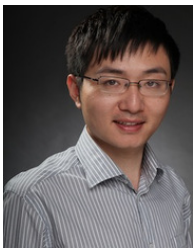

Shengqiang Cai *joined the Department of Mechanical and Aerospace Engineering at UCSD as an Assistant Professor in Nov. 2012. Before this, he was a postdoctoral fellow at Massachusetts Institute of Technology from 2011 to 2012. Dr. Cai earned his Ph.D. degree in Mechanical Engineering from Harvard University in 2011, after obtaining a Master's of Engineering and a Bachelor's of Science from University of Science and Technology of China. Dr. Cai's research interests mainly include mechanics of soft materials and structures, mechanics of biomaterials and three dimensional fabrication techniques.*

Falko Kuester *received an MS degree in Mechanical Engineering in 1994 and MS degree in Computer Science and Engineering in 1995 from the University of Michigan, Ann Arbor. In 2001 he received his PhD from the University of California, Davis and currently is the Calit2 Professor for Visualization and Virtual Reality at the University of California, San Diego. Dr. Kuester holds appointments as Associate Professor in the Departments of Structural Engineering and Computer Science and Engineering and serves as the director of the Calit2 Center of Interdisciplinary Science for Art, Architecture and Archaeology, CISA3.*